GEOLOGY

ISSN 0091-7613

JANUARY 2001 • VOL. 29 NO. 1 • P. 1–96

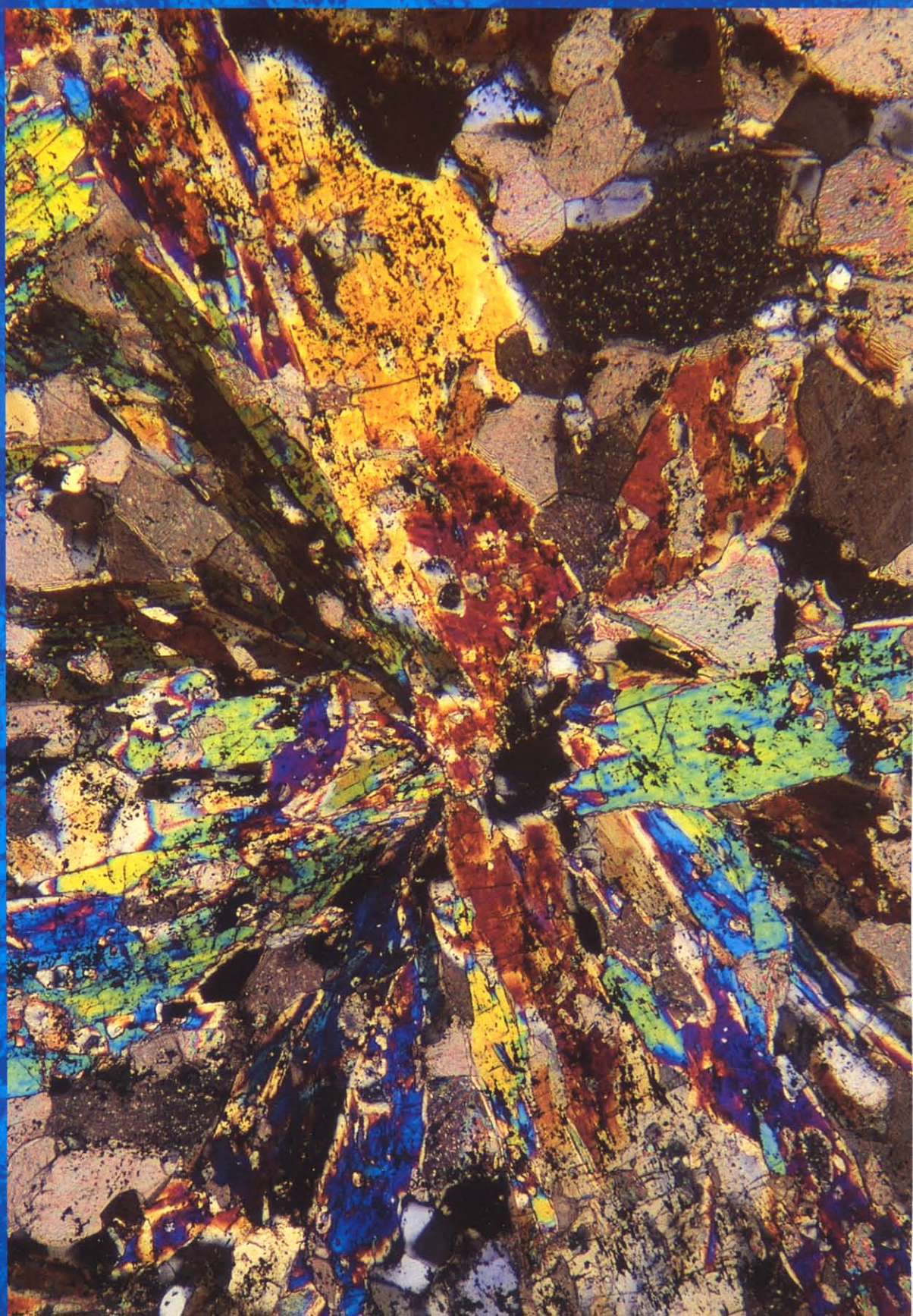

Release of CO_2 from carbonate rocks during regional metamorphism of lithologically heterogeneous crust

Jay J. Ague*
Department of Geology and Geophysics, Yale University, P.O. Box 208109, New Haven, Connecticut 06520-8109, USA

ABSTRACT

Prograde regional metamorphism drives CO_2 from carbonate rock to crustal fluids that ascend and ultimately interact with the atmosphere and oceans. The observed loss of CO_2 from metamorphic belts remains problematic, however, because the cooling that accompanies fluid ascent favors reactions that add CO_2 to metacarbonate rock by removing CO_2 from fluids. A new two-dimensional model of coupled mass transfer, chemical reaction, and heat transport was developed to assess how rock devolatilization proceeds along the upward escape paths of crustal fluids during prograde metamorphism. The model is based on upper greenschist to lower amphibolite facies growth of amphibole in metacarbonate layers and garnet and biotite in intercalated metapelite layers of the Wepawaug Schist, Connecticut (Acadian orogeny). The modeling indicates that during heating, CO_2 concentrations were larger in metacarbonate layers than in adjacent metapelite layers because amphibole growth in metacarbonates produced CO_2, whereas garnet and biotite growth in metapelites produced H_2O. The resulting cross-layer concentration gradients drove H_2O into the metacarbonate layers and CO_2 out by diffusion and the transverse component of mechanical dispersion. Such cross-layer mass transfer can continually force rock decarbonation while fluids ascend, dominating the effects of cooling, unless fluid fluxes are large and prograde heating rates are small. Consequently, prograde metamorphism of carbonate-bearing sedimentary sequences containing significant amounts of pelitic rock will release CO_2 to regionally migrating fluids in a wide range of orogenic settings, regardless of whether flow is in a direction of increasing or decreasing temperature. Regional CO_2 release can be driven by outcrop-scale processes of volatile exchange between contrasting lithologies.

Keywords: metamorphism, carbon dioxide, fluid flow, Connecticut, numerical modeling.

INTRODUCTION

The degassing of CO_2 from active orogens plays a fundamental role in Earth's carbon cycle and may be a major control on global climate (e.g., Kerrick and Caldeira, 1993; Selverstone and Gutzler, 1993; Berner, 1999; Ingebritsen and Manning, 1999). Metamorphic CO_2 fluxes may be as large as those through mid-ocean ridges and from volcanic arcs, but remain difficult to define and quantify. Proper understanding of degassing rates requires knowledge of how CO_2 is released from metacarbonate rocks during metamorphism and then transported upward through the crust. The Acadian orogen of the New England area of the United States exposes metacarbonate-bearing units for hundreds of kilometers along its strike, and provides an ideal field laboratory for examination of volatile mass transfer (e.g., Hewitt, 1973; Tracy et al., 1983; Ferry, 1994; Ague and van Haren, 1996). This paper focuses on the Wepawaug Schist, Connecticut, which underwent prograde metamorphism ca. 420–380 Ma (Lanzirotti and Hanson, 1996). Metamorphic grade increases from east to west from the Barrovian chlorite to kyanite zones; metacarbonate units within the formation progressively lost CO_2 with increasing metamorphic grade (Hewitt, 1973; Tracy et al., 1983; Palin, 1992; Ague and van Haren, 1996).

Chemical and oxygen isotopic evidence indicates that fluids flowed out of the higher grade parts of the Wepawaug Schist down regional temperature (T) and pressure (P) gradients during Acadian metamorphism (Ague, 1994; van Haren et al., 1996), consistent with recent models of orogenic fluid flow (Hanson, 1997). However, Baumgartner and Ferry (1991) showed that such flow down T gradients (down-T) should force common metacarbonate reactions to consume CO_2, at variance with the observed loss of CO_2 from the Wepawaug metacarbonate layers. Consider the common prograde reaction (1) 5 dolomite + 8 quartz + H_2O = tremolite + 3 calcite + 7 CO_2.

For a cooling fluid parcel flowing down-T through a rock mass composed only of metacarbonate, the mole fraction of CO_2 (X_{CO_2}) in the fluid decreases as T decreases because the reac-

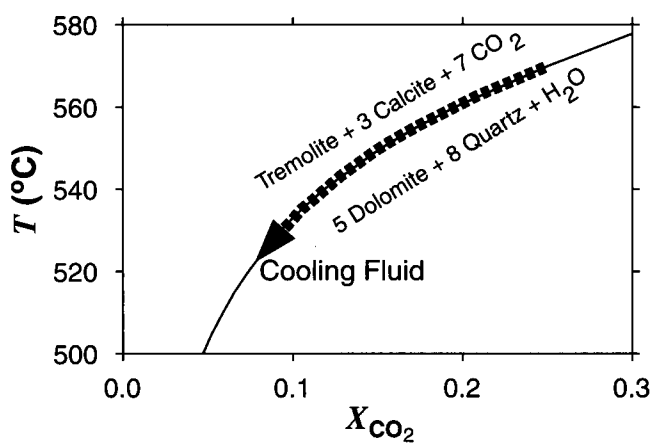

Figure 1. Equilibrium for reaction 1 at 7 kbar (thin line). X_{CO_2} is mole fraction CO_2 in fluid. Pressure and kinetic effects shift position of reaction (not shown), but trend of decreasing X_{CO_2} with decreasing temperature (T) would in general be preserved.

*E-mail: jay.ague@yale.edu.

Data Repository item 2000110 contains additional material related to this article.

tion proceeds to the left, consuming CO_2 (Fig. 1; cooling path). Conversely, fluid flowing in the direction of increasing T (up-T) would drive CO_2 release. Thus, much of the loss of CO_2 during prograde Acadian metamorphism has been attributed to up-T fluid flow (e.g., Ferry, 1994). However, in a heterogeneous rock package, transport of water from dehydrating metapelites into metacarbonate layers could also drive the reaction to the right, producing amphibole, if the resulting CO_2 was then lost to the surroundings (Hewitt, 1973; Ague and Rye, 1999). The key question is thus, can volatile exchange between layers drive prograde reaction and liberate CO_2 even when fluids are flowing out of an orogen, cooling while they ascend?

This question is addressed using a new two-dimensional numerical model of coupled mass and energy conservation incorporating Darcian fluid flow, anisotropic diffusion and mechanical dispersion, consumption and production of CO_2, H_2O, and heat by chemical reactions, heat transport by conduction and fluid flow, and radiogenic heat production.[1] The major goal is to derive general knowledge about devolatilization that is robust and independent of uncertainties on model parameters. The model is based on field observations and focuses on the simultaneous growth of amphibole in metacarbonate layers and garnet and biotite in metapelite layers, and widespread reaction relations in upper greenschist and lower amphibolite facies parts of the Wepawaug Schist and in much of northern New England (Ferry, 1994). Representative upper greenschist facies P-T conditions were used (Ague, 1994). External water-rich fluids derived from, for example, degassing magmas also drove rock decarbonation, particularly in the kyanite zone (Tracy et al., 1983; Palin, 1992; Ague, 1994; van Haren et al., 1996); these processes are not considered herein.

[1]GSA Data Repository item 2000110, Model description, is available on request from Documents Secretary, GSA, P.O. Box 9140, Boulder, CO 80301-9140, editing@geosociety.org, or at www.geosociety.org/pubs/ft2000.htm.

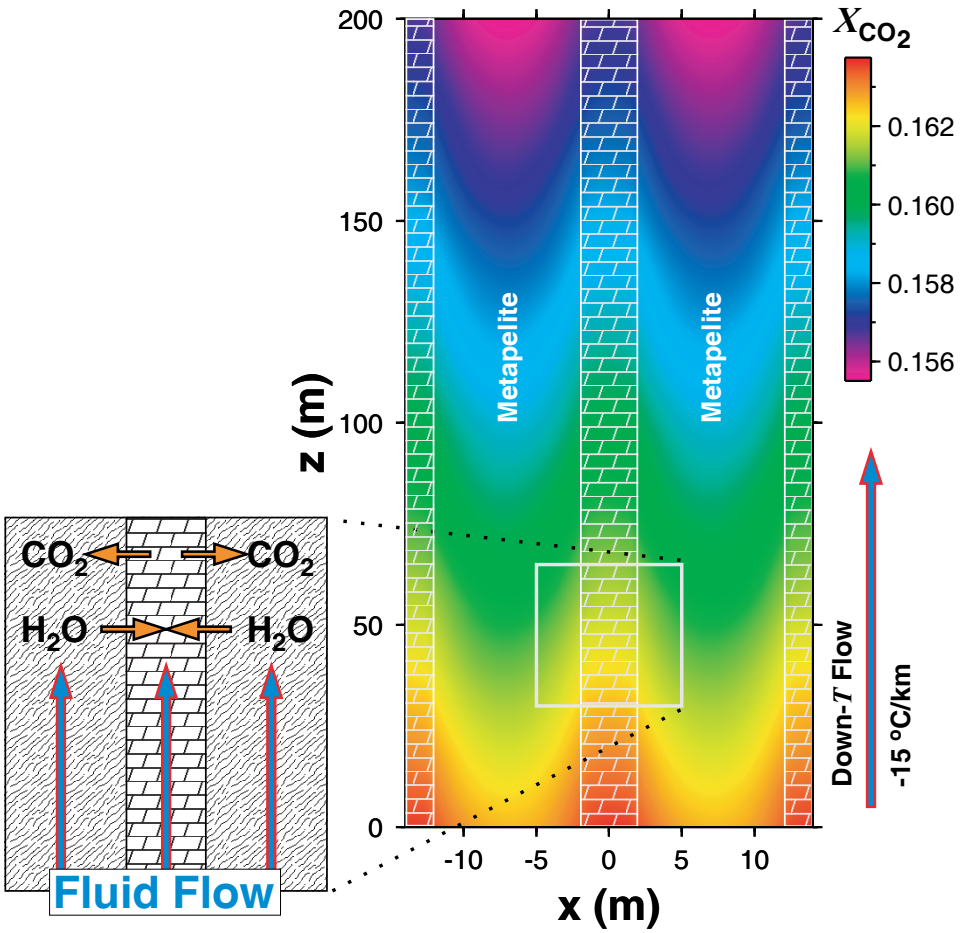

Figure 2. Contours of mole fraction CO_2 (X_{CO_2}) for intercalated metacarbonate layers (brick pattern) and metapelite layers after 2 × 10^5 model yr; temperature (T) is increasing at 15 °C/m.y., and fluid flow velocity = 100 km/m.y. Pressure and temperature decrease upward (increasing z) in direction of flow. X_{CO_2} is larger in metacarbonate layers than in adjacent metapelite layers because amphibole growth in metacarbonate produces CO_2 whereas garnet and biotite growth in metapelite produces H_2O. Cross-layer transport of H_2O into, and CO_2 out of, metacarbonate layers occurs by diffusion and transverse component of mechanical dispersion (orange arrows in inset diagram), driving further amphibole growth and CO_2 loss. For all simulations, fluid was input into base of system with boundary concentration gradients specified by local equilibrium with dolomite + quartz + tremolite + calcite. Note exaggeration of horizontal scale on contour map.

TRANSPORT

Anisotropic fluid flow parallel to planar rock fabrics appears to have been dominant in metasedimentary sequences over large regions of New England (Ferry, 1994) and elsewhere (e.g., Rye et al., 1976). In the Wepawaug Schist, schistosity and relic sedimentary bedding dip steeply due to premetamorphic to synmetamorphic folding (cf. Ague, 1994). Thus, fluid flow up and out of the rock would have been largely layer parallel. This situation is modeled using vertical intercalated metacarbonate and metapelite layers, with fluid flow upward in the positive z direction (Fig. 2); other orientations are also discussed in the following. In the field, the metacarbonate layers are widely spaced and range from a few centimeters to as much as 10 m thick; most are <5 m thick. Both 1- and 4-m-thick layers are modeled, separated by 10-m-thick metapelite layers, yielding volume percent metacarbonate values of ~9% and ~29%, consistent with observations.

Diffusion and mechanical dispersion are collectively termed hydrodynamic dispersion. The effective diffusion coefficient for porous solids is defined as the product of the: (1) diffusion coefficient for fluid species; (2) tortuosity of the interconnected, fluid-filled pore space; and (3) porosity. A typical fluid species diffusion coefficient of 1×10^{-8} m^2/s was used (cf. Ague, 1998). Transport pathways are likely to be the least tortuous parallel to the platy phyllosilicate grains that define rock fabrics. Tortuosity values measured in porous materials typically range from ~0.3 for tortuous pathways, to ~0.64 for less tortuous ones (Bear, 1972). On this basis, values of 0.3 and 0.64 were adopted for diffusion perpendicular to and parallel to layering, respectively. Initial porosity was set to a small, representative value of 0.001 (e.g., Hanson, 1997), but the model also includes reversible changes in porosity and permeability due to fluid pressure variations (Ague and Rye, 1999). Mechanical dispersion accompanies advection and acts to smear out concentration fronts both parallel (longitudinal) and perpendicular (transverse) to the flow direction (Bear, 1972). Low-permeability shales, perhaps the best analogs for low-permeability metamorphic rocks, have longitudinal dispersivities ranging from near 0 m to ~10 m (cf. Garven and Freeze, 1984). An intermediate value of 5 m was used herein. Transverse dispersivity was set to 0.5 m because it is typically an order of magnitude or more smaller than longitudinal dispersivity (Garven and Freeze, 1984).

Fluid pressure (P_f) gradients near lithostatic (Hanson, 1997; Ingebritsen and Manning, 1999) and geothermal gradients of –15 to –20 °C/km (Hanson, 1997) are probably widespread over large sections of the middle and lower crust dur-

ing continental collision. The initial P_f gradient was set to lithostatic, and P_f was 7 kbar at the base of the system (z = 0 m). P_f at the base and top (z = 200 m) of the system remained constant at their initial values. Initial T = 550 °C at z = 0 m, and initial T gradients were either –15 or –20 °C/km. Heating was simulated by increasing the T at the base and top boundaries at prescribed rates. No mass or heat fluxes were allowed across the sides of the system. Thermal conductivity = 5 W/(m·K) and radiogenic heat production = 3 μW/m^3 (cf. Garven and Freeze, 1984; Hanson, 1997). P_f and T were allowed to evolve freely within the flow region. T gradients were always within ~±1 °C/km of initial values because of the relatively large thermal conductivity of rocks.

A two order of magnitude range of upward fluid flow velocities (1–100 cm/yr, or 10–1000 km/m.y.) was examined by adjusting the permeability of the flow region, yielding fluxes in the range thought typical for regional metamorphism (e.g., Hanson, 1997; Ingebritsen and Manning, 1999). Fluid viscosity was fixed at 1.15×10^{-4} Pa·s (e.g., Baumgartner and Ferry, 1991).

CHEMICAL REACTION

Natural amphibole and dolomite contain significant iron (Hewitt, 1973). However, solid-solution effects will not displace the equilibrium relations for the Mg–end-member reaction 1 a great deal because there are only two Mg-Fe phases involved; the phases are reasonably described by ideal mixing (Ferry, 1994); and both phases have similar Mg/Fe. Thus, the thermodynamic properties of the Mg–end-member reaction were used.

Muscovite and chlorite reacted to form garnet and biotite in the metapelitic layers of the Wepawaug Schist during prograde metamorphism (van Haren et al., 1996). Three linearly independent reactions can be written to relate P, T, and mineral and fluid chemistry among quartz (Qtz), muscovite (Ms), almandine-pyrope (Alm-Prp), annite-phlogopite (Ann-Phl), clinochlore-daphnite (Chl-Dph), and fluid. Based on van Haren et al. (1996), excellent models for prograde garnet growth are the Fe and Mg–end-member reactions: (2) 3 Dph + Ms + 3 Qtz = Ann + 4 Alm + 12 H_2O and (3) 3 Chl + Ms + 3 Qtz = Phl + 4 Prp + 12 H_2O. Fe-Mg exchange links the two reactions and was modeled by: (4) Alm + Phl = Ann + Prp. Garnet, biotite, and chlorite were treated as ideal Fe-Mg solid solutions that were compositionally homogeneous over each step of reaction progress; quartz and muscovite were treated as pure phases. Chemical zonation in garnet has a negligible impact on the results for the relatively small T increases examined.

The model used internally consistent thermodynamic data (Berman, 1991; Holland and Powell, 1998; see footnote 1) and nonideal CO_2-H_2O fluids (Kerrick and Jacobs, 1981). A linear rate model was used for reaction kinetics (Lasaga and Rye, 1993; Ague, 1998); varying rate parameters within reasonable limits changes the details of the results, but not the general conclusions.

RESULTS AND DISCUSSION

The simulations started with local fluid-rock equilibrium throughout the system. Heating and fluid advection were then initiated, simulating prograde metamorphism in a flow field.

X_{CO_2} in the metacarbonate layers decreases down-T in the direction of flow (Fig. 2), as expected for reaction 1 (Fig. 1). X_{CO_2} is larger in the metacarbonate layers than in adjacent metapelite layers because amphibole growth in the metacarbonate produces CO_2, whereas garnet and biotite growth in the metapelite produces H_2O. Hydrodynamic dispersion drives mass transfer from regions of high concentration to regions of low concentration. Consequently, CO_2 is transported out of and H_2O is transported into the metacarbonate units across layering by diffusion and the transverse component of dispersion (Fig. 2), driving amphibole growth and CO_2 loss even though fluids are ascending and cooling. Concentration gradients across adjacent metacarbonate and metapelite layers are predicted to be small (Fig. 2).

Down-T advection tends to drive reaction 1 to the left, consuming CO_2 (Fig. 1). Decreasing the magnitude of the T gradient in the direction of flow decreases the rate of CO_2 consumption along the flow path (Baumgartner and Ferry, 1991), thus reducing the importance of down-T advection relative to cross-layer hydrodynamic dispersion (Fig. 3).

The T gradient in the direction of flow that influences reaction progress need not coincide with the geothermal gradient. For example, if fluids move toward the surface parallel to layering at 45° to a vertical geothermal gradient of –21 °C/km, the T gradient in the direction of flow is only –15 °C/km. Reaction progress systematics would be the same as shown in Figure 3 (A and C). In general, the thermal effects on reaction are greatest when the geothermal gradient and the flow direction are parallel, are reduced as they diverge, and are eliminated when they are perpendicular.

Reducing the fluid velocity and flux reduces the importance of down-T advection relative to cross-layer hydrodynamic dispersion such that decreased down-T flow enhances prograde reaction and CO_2 loss from metacarbonate layers (Fig. 3).

Larger heating rates increase the rates of H_2O and CO_2 release, the magnitudes of lateral concentration gradients, and thus the importance of

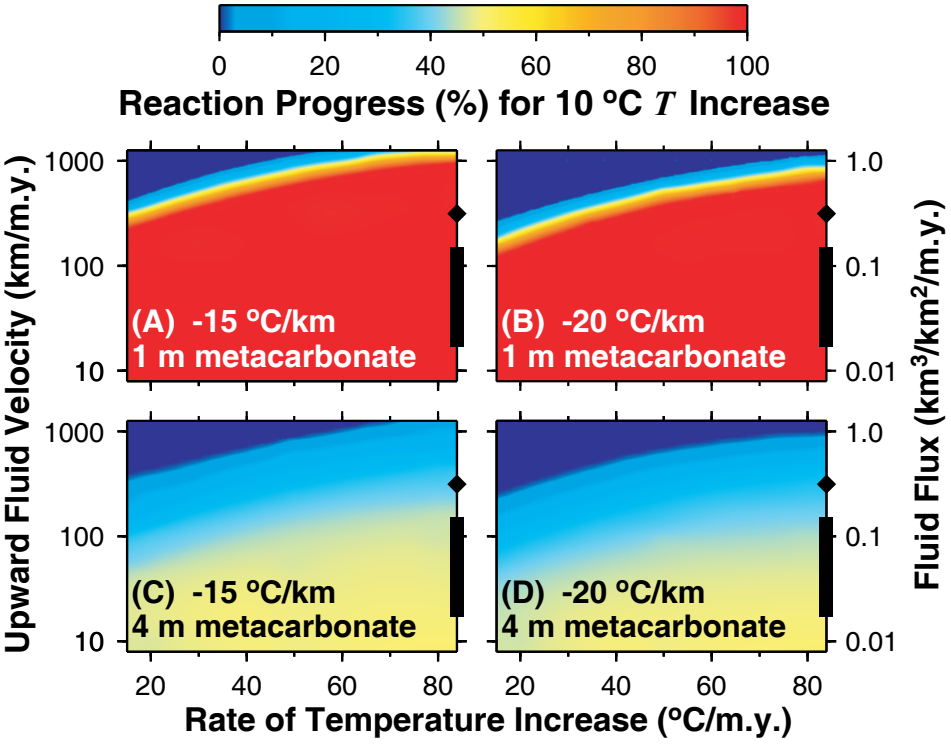

Figure 3. Average progress of reaction 1 for 10 °C temperature (T) increase. Initial metacarbonate rock contains 10 volume% dolomite (maximum likely available) and representative amounts of quartz, calcite, and biotite based on middle greenschist facies field relations in Wepawaug Schist. 100% reaction progress corresponds to complete destruction of dolomite and maximum production of amphibole; 0% corresponds to no prograde reaction. Range of peak metamorphic fluxes from Hanson (1997, his Figs. 5–7) is shown as black bar on right flux axes; flux of Ingebritsen and Manning (1999) is shown by black diamond. Reaction progress increases with (1) decreased fluid velocity and flux; (2) decreased magnitude of T gradient along flow path (fluid flow is down T); and (3) increased heating rate. Thick (4 m) layers are large reservoirs of reactant dolomite and thus have smaller percentage reaction progress than 1 m layers for same amount of reaction time.

cross-layer hydrodynamic dispersion relative to down-T advection (Fig. 3).

Dolomite destruction and amphibole growth are complete (100% reaction progress) in 1-m-thick layers for most heating and flow rates, even for T increases of as little as 10 °C (Fig. 3). Thick metacarbonate layers are large reservoirs of reactant dolomite and quartz and thus they take longer to react than thin layers (Fig. 3, C and D). However, the total amount of CO_2 released over a given T-time interval is nearly identical for 1- and 4-m-thick layers.

Cross-layer advection occurs if the layers are at an angle to the flow direction, although the effect on reaction progress is small if the angle is small. For example, tilting 4-m-thick metacarbonate layers and intercalated metapelite layers ~10° away from the vertical flow direction changes reaction progress by <2% relative to the case of vertical layering for Ingebritsen and Manning's (1999) fluid flux of 10^{-11} $m^3/m^2/s$ (not illustrated).

In summary, prograde amphibole growth and CO_2 production are enhanced as the magnitudes of the fluid flux and/or T gradient along the down-T flow direction decrease, and as the heating rate increases (Fig. 3).

CONCLUSIONS

Loss of CO_2 from metacarbonate rocks depends critically on (1) regional-scale gradients in fluid composition due to changes in P and T along crustal flow paths; and (2) local, outcrop-scale gradients between contrasting lithologies due to production of different fluids during prograde reaction. Regional down-T ascent and cooling of fluids along lithologic layering favors retrograde reaction, sequestering CO_2 in metacarbonate rocks. However, devolatilization reactions tend to produce larger CO_2 concentrations in metacarbonate layers than in adjacent metapelitic layers such that cross-layer concentration gradients drive H_2O into metacarbonate layers and CO_2 out by diffusion and the transverse component of mechanical dispersion (Fig. 2). For metapelite-dominated sequences like the Wepawaug Schist, this cross-layer transport forces prograde decarbonation even while fluids ascend and cool, unless fluid fluxes are large or prograde heating rates are small (Fig. 3). The flux of CO_2 decreases upward along the flow path as CO_2 produced by reaction is diluted by water from dehydrating schists. Reaction progress for Wepawaug metacarbonate layers increases near lithologic contacts (Hewitt, 1973), strongly suggesting an important role for cross-layer volatile exchange. Differences in amounts of CO_2 loss from one metacarbonate layer to the next in outcrop will result not only from local variations in fluid flow, but also from variations in fluid composition and fluid production rates in neighboring layers poorer in carbonate minerals. Reactions that add CO_2 to rocks, enhancing crustal carbon storage, are favored if cooling fluids escape upward through thick metacarbonate sequences lacking significant metapelite or other sources of H_2O. The results emphasize that field estimation of crustal fluid flow paths and fluxes requires consideration of advection and hydrodynamic dispersion in more than one space dimension (e.g., Skelton et al., 1995; Ague and Rye, 1999).

ACKNOWLEDGMENTS

I thank E.W. Bolton and D.M. Rye for thoughtful discussions, and C.P. Chamberlain and an anonymous referee for critical reviews. Supported by National Science Foundation grant EAR-9706638.

REFERENCES CITED

Ague, J.J., 1994, Mass transfer during Barrovian metamorphism of pelites, south-central Connecticut, II: Channelized fluid flow and the growth of staurolite and kyanite: American Journal of Science, v. 294, p. 1061–1134.

Ague, J.J., 1998, Simple models of coupled fluid infiltration and redox reactions in the crust: Contributions to Mineralogy and Petrology, v. 132, p. 180–197.

Ague, J.J., and Rye, D.M., 1999, Simple models of CO_2 release from metacarbonates with implications for interpretation of directions and magnitudes of fluid flow in the deep crust: Journal of Petrology, v. 40, p. 1443–1462.

Ague, J.J., and van Haren, J.L.M., 1996, Assessing metasomatic mass and volume changes using the bootstrap, with application to deep-crustal hydrothermal alteration of marble: Economic Geology, v. 91, p. 1169–1182.

Baumgartner, L.P., and Ferry, J.M., 1991, A model for coupled fluid flow and mixed-volatile mineral reactions with applications to regional metamorphism: Contributions to Mineralogy and Petrology, v. 106, p. 273–285.

Bear, J., 1972, Dynamics of fluids in porous media: New York, Elsevier, 764 p.

Berman, R.G., 1991, Thermobarometry using multi-equilibrium calculations: A new technique, with petrological applications: Canadian Mineralogist, v. 29, p. 833–855.

Berner, R.A., 1999, A new look at the long-term carbon cycle: GSA Today, v. 9, no. 11, p. 1–6.

Ferry, J.M., 1994, Overview of the petrologic record of fluid flow during regional metamorphism in northern New England: American Journal of Science, v. 294, p. 905–988.

Garven, G., and Freeze, A.R., 1984, Theoretical analysis of the role of groundwater flow in the genesis of stratabound ore deposits. 2. Quantitative results: American Journal of Science, v. 284, p. 1085–1174.

Hanson, R.B., 1997, Hydrodynamics of regional metamorphism due to continental collision: Economic Geology, v. 92, p. 880–891.

Hewitt, D.A., 1973, The metamorphism of micaceous limestones from south-central Connecticut: American Journal of Science, v. 273-A, p. 444–469.

Holland, T.J.B., and Powell, R., 1998, An internally consistent thermodynamic data set for phases of petrological interest: Journal of Metamorphic Geology, v. 16, p. 309–343.

Ingebritsen, S.E., and Manning, C.E., 1999, Geological implications of a permeability-depth curve for the continental crust: Geology, v. 27, p. 1107–1110.

Kerrick, D.M., and Caldeira, K., 1993, Paleoatmospheric consequences of CO_2 released during early Cenozoic regional metamorphism in the Tethyan orogen: Chemical Geology, v. 108, p. 201–230.

Kerrick, D.M., and Jacobs, G.K., 1981, A modified Redlich-Kwong equation for H_2O, CO_2, and H_2O-CO_2 mixtures at elevated temperatures and pressures: American Journal of Science, v. 281, p. 735–767.

Lanzirotti, A., and Hanson, G.N., 1996, Geochronology and geochemistry of multiple generations of monazite from the Wepawaug Schist, Connecticut, USA: Implications for monazite stability in metamorphic rocks: Contributions to Mineralogy and Petrology, v. 125, p. 332–340.

Lasaga, A.C., and Rye, D.M., 1993, Fluid flow and chemical reaction kinetics in metamorphic systems: American Journal of Science, v. 293, p. 361–404.

Palin, J.M., 1992, Petrologic and stable isotopic studies of the Wepawaug Schist, Connecticut [Ph.D. thesis]: New Haven, Connecticut, Yale University, 170 p.

Rye, R.O., Schuiling, R.D., Rye, D.M., and Jansen, J.B.H., 1976, Carbon, hydrogen and oxygen isotope studies of the regional metamorphic complex at Naxos, Greece: Geochimica et Cosmochimica Acta, v. 40, p. 1031–1049.

Selverstone, J., and Gutzler, D.S., 1993, Post-125 Ma carbon storage associated with continent-continent collision: Geology, v. 21, p. 885–888.

Skelton, A.D.L., Graham, C.M., and Bickle, M.J., 1995, Lithological and structural controls on regional 3-D fluid flow patterns during greenschist facies metamorphism of the Dalradian of the SW Scottish Highlands: Journal of Petrology, v. 36, p. 563–586.

Tracy, R.J., Rye, D.M., Hewitt, D.A., and Schiffries, C.M., 1983, Petrologic and stable-isotopic studies of fluid-rock interactions, south-central Connecticut: I. The role of infiltration in producing reaction assemblages in impure marbles: American Journal of Science, v. 283A, p. 589–616.

van Haren, J.L.M., Ague, J.J., and Rye, D.M., 1996, Oxygen isotope record of fluid infiltration and mass transfer during regional metamorphism of pelitic schist, south-central Connecticut, USA: Geochimica et Cosmochimica Acta, v. 60, p. 3487–3504.

Manuscript received March 31, 2000
Revised manuscript received September 13, 2000
Manuscript accepted September 15, 2000

RELEASE OF CO_2 FROM CARBONATE ROCKS DURING REGIONAL METAMORPHISM OF LITHOLOGICALLY HETEROGENEOUS CRUST

Model Description for GSA Data Repository

This supplemental material describes the 2–D numerical model used to compute mass transfer, heat transfer, and chemical reaction. Values for model variables not described here are presented in the main text. Further discussion of many of the concepts involved can be found in the 1–D studies of Ague (1998) and Ague and Rye (1999).

CONSERVATION OF MASS

Conservation of mass for species i (CO_2 or H_2O) in a multicomponent fluid for a fully–saturated, porous flow region is given by the advection-dispersion-reaction equation (cf. Bear, 1972; Garven and Freeze, 1984; Ague and Rye, 1999):

$$\frac{\partial (\phi C_i)}{\partial t} = \nabla \cdot \left(\phi \tilde{D}_i \nabla C_i\right) - \nabla \cdot (\phi \boldsymbol{v} C_i) + \phi \sum_j R_{i,j} \tag{1}$$

in which t is time; C is concentration; $\boldsymbol{v}$ is the pore fluid velocity vector; $\tilde{D}$ is the hydrodynamic dispersion tensor incorporating the effects of both molecular diffusion (including tortuosity) and mechanical dispersion; ϕ is porosity; and $R_{i,j}$ is the production rate (positive) or consumption rate (negative) of i due to chemical reaction j. The three terms on the right hand side of the equation account for hydrodynamic dispersion, advection, and chemical reaction, respectively. The 2–D version of equation (1) was solved with x horizontal and z vertical (increasing upwards). Diffusion of H_2O and CO_2 through the solids was assumed negligible relative to transport in the fluid phase.

The principal components of the tortuosity and mechanical dispersion tensors are parallel to the x and z coordinate axes, and nearly all fluid flow is upwards, parallel to z. Consequently, the hydrodynamic dispersion tensor can be written in terms of the two nonzero

components (Bear, 1972):

$$D_{zz,i} = \alpha_{L,i}|v_z| + D_{f,i}\tau_{zz}, \tag{2}$$

$$D_{xx,i} = \alpha_{T,i}|v_z| + D_{f,i}\tau_{xx}, \tag{3}$$

in which $D_{zz,i}$ and $D_{xx,i}$ are the components of the tensor in the z and x directions, respectively; $\alpha_{L,i}$ and $\alpha_{T,i}$ are the coefficients of longitudinal and transverse dispersivity, respectively; $|v_z|$ is the absolute value of the pore fluid velocity in the z direction; $D_{f,i}$ is the diffusion coefficient for species i in pure fluid; and τ_{zz} and τ_{xx} are the z and x components of the tortuosity tensor. Off-diagonal terms (e.g., $D_{xz,i}$) are zero.

Reaction rates were treated using the general kinetic model of Lasaga and Rye (1993), as modified by Ague (1998) to account for stoichiometric coefficients other than unity and both positive and negative Gibbs free energy changes of reaction:

$$R_{i,j} = \left(\frac{1}{\phi}\right) k_j \nu_{i,j} \bar{A}_{l,j} s |\Delta G_j|^{n_j} \tag{4}$$

in which k_j is the intrinsic reaction rate constant for reaction j; $\nu_{i,j}$ is the stoichiometric coefficient of species i in reaction j; $\bar{A}_{l,j}$ is the surface area exposed to fluid of the rate–limiting mineral l in reaction j; $|\Delta G_j|$ is the absolute value of the Gibbs free energy change of reaction j at the T and P of interest; n_j is the reaction order for reaction j; and s is, by convention, +1 if ΔG_j is negative and -1 otherwise. The net production/consumption rate for i is obtained by summing over the rate expressions for all reactions j (third term on right of equation [1]). k_j has an Arrhenius–type T–dependence (e.g., Oxtoby et al., 1999):

$$k_j = k_j^o \exp\left(\frac{-Ea_j}{R}\left(\frac{1}{T} - \frac{1}{T^o}\right)\right) \tag{5}$$

in which k_j^o is the intrinsic reaction rate constant at some convenient reference temperature

T^o; Ea_j is the activation energy for reaction j; and R is the gas constant. This paper uses values for linear kinetics: $n_j = 1$; $k_j^o = 3.33 \times 10^{-20}$ (mol/m^2/s) (J/mol)$^{-1}$; $T^o = 873.15$ K (600 °C); $Ea_j = 83.68$ kJ/mole (Lasaga and Rye, 1993). Reaction stoichiometries were adjusted to yield 14 oxygens on the product and reactant sides, consistent with the reaction studied by Schramke et al. (1987) which forms the basis for the linear kinetic model parameters used herein. The rate–limiting reactive surface area was set to a representative value of 100 m^2/m^3 (Ague and Rye, 1999); Ague (1998) discusses varying surface areas. The change in moles for a solid phase θ due to reaction is (Ague, 1998; Ague and Rye, 1999):

$$\frac{\partial m_{\theta,j}}{\partial t} = k_j \nu_{\theta,j} \bar{A}_{l,j} s |\Delta G_j|^{n_j} \tag{6}$$

in which m_θ is the moles of θ per unit volume of rock. For the model problem, the main effect of varying kinetic rate parameters is to change the shape of reaction fronts. When reaction rates are slow relative to mass transport rates, fronts tend to be broad, whereas faster reaction produces sharper fronts. Detailed examples and discussion of these rate effects can be found in Ague (1998) and Ague and Rye (1999).

The fluid flux vector, $\boldsymbol{q}$, is related to pore fluid pressure (P_f) by Darcy's law, written here for a vertical z-axis:

$$\boldsymbol{q} = -\frac{\tilde{\kappa}}{\mu} \left(\nabla P_f - \rho_f \boldsymbol{g} \right) \tag{7}$$

in which $\tilde{\kappa}$ is the permeability tensor; μ is the fluid viscosity; and $\boldsymbol{g}$ is the acceleration of gravity. The pore velocity $\boldsymbol{v}$ is given by $\boldsymbol{v} = \boldsymbol{q}/\phi$. Porosity change has reversible and irreversible components (Walder and Nur, 1984):

$$\frac{\partial \phi}{\partial t} = \phi \beta_\phi \left(\frac{\partial P_f}{\partial t} \right) + \left(\frac{\partial \phi}{\partial t} \right)_{Irrev} \tag{8}$$

in which β_ϕ is a "pore compressibility" for the rock matrix. The first term on the right

accounts for reversible expansion or collapse of pore space related to changes in P_f and is the only term considered here (cf. Ague and Rye, 1999). The isothermal compressibility of H_2O at 550 °C and 7000 bars is $\sim 3 \times 10^{-5}$ bar^{-1} (Kerrick and Jacobs, 1981); β_ϕ is currently poorly known but was set to 1×10^{-5} bar^{-1} under the assumption that the rock matrix is less compressible than the fluid. Changes in permeability due to reversible changes in ϕ were small in the models and were calculated following Ague and Rye (1999).

CONSERVATION OF ENERGY

The conservation of energy equation used in the model is given by:

$$\rho_r C_{P,r} \frac{\partial T}{\partial t} = -\nabla \cdot (\boldsymbol{q} \rho_f C_{P,f} T) + \nabla \cdot (K_T \nabla T) + A - \phi \sum_j \Delta H_{r,j} R_j \tag{9}$$

in which ρ_r is the density of rock (rock = solids + pore fluid); $C_{P,r}$ is the heat capacity of rock; T is temperature; $\boldsymbol{q}$ is the fluid flux vector; ρ_f is the density of fluid; $C_{P,f}$ is the heat capacity of fluid; K_T is the thermal conductivity of rock; A is the rate of heat generation by radioactive decay; ϕ is porosity; $\Delta H_{r,j}$ is the enthalpy change for reaction j; and R_j is the overall rate of reaction j. The four terms on the right hand side of the equation account for fluid advection, conduction, radiogenic heat production, and chemical reaction, respectively. The negative sign in front of the reaction term accounts for the thermodynamic convention that exothermic reactions have negative ΔH_r, and vice versa. For the limited range of T and fluid composition used in the models, several properties were treated as constants: ρ_r = 2800 kg/m^3; $C_{P,r}$ = 1046 J/kg/K; $\rho_f C_{P,f} = 3.5 \times 10^6$ J/m^3/K (Brady, 1988). The overall rate for reaction j is:

$$R_j = \left(\frac{1}{\phi}\right) k_j \bar{A}_{l,j} s |\Delta G_j|^{n_j}. \tag{10}$$

THERMODYNAMIC DATA

Most thermodynamic data were taken from Berman (1991), and non-ideal H_2O–CO_2 fluids were treated following Kerrick and Jacobs (1981). The data set of Berman (1991) lacks data for the Fe–chlorite end member daphnite (Dph). Thermodynamic data for Dph internally–consistent with Berman (1991) were estimated based on the data set of Holland and Powell (1998). The positions of the following two univariant reactions were computed using the data set of Holland and Powell (1998): i) 3 Daphnite + Muscovite + 3 Quartz = Annite + 4 Almandine + 12 H_2O; and ii) 3 Daphnite + 5 Muscovite = 8 Kyanite + 5 Annite + Quartz + 12 H_2O. This calculation is referred to as "Method I". The same reactions were also calculated using the Holland and Powell (1998) data set for Dph, the Berman (1991) data set for all other solids, and the fugacity relations of Kerrick and Jacobs (1981) ("Method II"). Under the assumption that the univariant curves computed using Method I were "correct", the standard enthalpy and Gibbs free energy of formation for Dph for the Method II calculation were adjusted slightly to bring the Method II results into agreement with those for Method I. The optimum adjustment was -4 kJ/mol, well within the 2σ uncertainties cited by Holland and Powell (1998).

NUMERICAL SOLUTION

The numerical model is a 2–D explicit finite difference scheme solved on a fixed cartesian grid. Hydrodynamic dispersion and heat conduction are treated using the Forward–Time, Centered–Space method (e.g., Press et al., 1992; Thomas, 1995), whereas advective mass and heat transfer are solved using Barton's method (Centrella and Wilson, 1984; Hawley et al., 1984; Ague, 1998; Ague and Rye, 1999) adopted herein to two space dimensions. Barton's method minimizes many of the numerical dispersion and dissipation problems inherent in other methods.

For each time step, the model first solves for conservation of energy (equation [9]) using values for the reaction term and fluid fluxes from the previous time step. Next, mass transfer

by advection and hydrodynamic dispersion, coupled to chemical reaction, are computed (equation [1]). Mass transfer and reaction are numerically coupled using operator splitting (e.g., Wilson, 1979; Hawley et al., 1984; Ague 1998; Ague and Rye, 1999). New fluid mole fractions, densities, and molar volumes are then calculated for each node in the grid based on the changes in fluid composition dictated by the transport–reaction relations. The new fluid pressures and molar volumes of CO_2 and H_2O are next solved for iteratively for each node using the known T, fluid molar volume, and mole fractions. The new porosities and permeabilities to be used in the next time step are then computed based on the changes in fluid pressure. Finally, the new fluid pressure and permeability distributions are used with Darcy's law (equation [7]) to compute fluxes throughout the flow region. These fluxes are input into the next time step to solve for advection–related heat and mass transport. Time steps are small enough (10^{-2}–10^{-3} yr) that the separation of the heat and mass transfer calculations has no significant impact on the results. Grid spacings in the x and z directions were varied in the ranges 0.25–1.0 m and 10–50 m, respectively, depending on the degree of spatial resolution desired.

MODEL VERIFICATION

Several methods were used to assess model performance. First, numerical transport algorithms were tested separately in the x and z directions by comparison with well–known 1-D solutions for nonreactive advective–dispersive transport (e.g., Fried and Combarnous, 1971).

Second, the temporal evolution of pore pressure for a variety of constant rates of water production and porosity change was tested against the solutions of Wong et al. (1997; equations 5, 6).

Third, the model was tested against the closed–form, 1-D, local–equilibrium, advection–reaction equation of Baumgartner and Ferry (1991) for the reaction: 5 Dolomite + 8 Quartz + H_2O = Tremolite + 3 Calcite + 7 CO_2. In order to be consistent with the Baumgartner

and Ferry (1991) equation, the test simulation was done using constant porosity, permeability, T, and P; constant T gradient (-20 °C/km , down–T flow); constant P gradient (lithostatic); constant flow rate (5×10^{-4} m^3/m^2/yr); and no heat production/consumption. The simulation was run for a total model time of 10^5 yr, yielding a time–integrated fluid flux of 50 m^3/m^2. The reaction progress for the simulation was then input into the Baumgartner and Ferry (1991) expression to calculate a time–integrated fluid flux with the same T, P, T gradient, and P gradient used in the numerical model. The numerical model time–integrated flux agrees with the Baumgartner and Ferry (1991) result to within 0.1 %—an excellent level of agreement. This is a particularly stringent test of Barton's method since modeling of pure advective mass transfer can be subject to many pathologies, particularly numerical dissipation and dispersion.

Finally, additional verification was done by evaluating fluid mass balances and by varying time steps and grid spacing.

REFERENCES

Ague, J. J., 1998, Simple models of coupled fluid infiltration and redox reactions in the crust: Contributions to Mineralogy and Petrology, v. 132, p. 180-197.

Ague, J. J., and Rye, D. M., 1999, Simple models of CO_2 release from metacarbonates with implications for interpretation of directions and magnitudes of fluid flow in the deep crust: Journal of Petrology, v. 40, p. 1443-1462.

Baumgartner, L. P., and Ferry, J. M., 1991, A model for coupled fluid flow and mixed-volatile mineral reactions with applications to regional metamorphism: Contributions to Mineralogy and Petrology, v. 106, p. 273-285.

Bear, J., 1972, Dynamics of Fluids in Porous Media, New York: Elsevier, 764 pp.

Berman, R. G., 1991, Thermobarometry using multi–equilibrium calculations: A new technique, with petrological applications: Canadian Mineralogist, v. 29, p. 833-855.

Centrella, J., and Wilson, J. R., 1984, Planar numerical cosmology. II. The difference equa-

tions and numerical tests: Astrophysical Journal Supplement Series, v. 54, p. 229-249.

Fried, J. J., and Combarnous, M. A., 1971, Dispersion in porous media. In Chow, V. T. (ed) Advances in Hydroscience, v. 7: Academic Press, New York, p. 170-282.

Garven, G., and Freeze, A.R., 1984, Theoretical analysis of the role of groundwater flow in the genesis of stratabound ore deposits. 1. Mathematical and numerical model: American Journal of Science, v. 284, p. 1085-1124.

Hawley, J. F., Smarr, L. L., and Wilson, J. R., 1984, A numerical study of nonspherical black hole accretion. II. Finite differencing and code calibration: Astrophysical Journal Supplement Series, v. 55, p. 211-246.

Holland, T. J. B., and Powell, R., 1998, An internally consistent thermodynamic data set for phases of petrological interest: Journal of Metamorphic Geology, v. 16, p. 309-343.

Kerrick, D. M., and Jacobs, G. K., 1981, A modified Redlich–Kwong equation for H_2O, CO_2, and H_2O–CO_2 mixtures at elevated temperatures and pressures: American Journal of Science, v. 281, p. 735-767.

Lasaga, A. C., and Rye, D. M., 1993, Fluid flow and chemical reaction kinetics in metamorphic systems: American Journal of Science, v. 293, p. 361-404.

Oxtoby, D. W., Gillis, H. P., and Nachtrieb, N. H., 1999, Principles of Modern Chemistry (4th ed.), Fort Worth: Saunders College, 876 p.

Press, W. H., Teukolsky, S. A., Vetterling, W. T. and Flannery, B. P., 1992, Numerical Recipes in FORTRAN (2nd ed.), New York: Cambridge University Press, 963 pp.

Schramke, J. A., Kerrick, D. M., and Lasaga, A. C., 1987, The reaction muscovite + quartz = andalusite + K-feldspar + water. Part I. Growth kinetics and mechanism: American Journal of Science, v. 287, p. 517-559.

Thomas, J. W., 1995, Numerical Partial Differential Equations: Finite Difference Methods, New York: Springer, 437 p.

Wilson, J. R., 1979, A numerical method for relativistic hydrodynamics. In Smarr LL (ed)

Sources of gravitational radiation: Cambridge University Press, New York, p. 423-445.

Wong, T., Ko, S. and Olgaard, D. L., 1997, Generation and maintenance of pore pressure excess in a dehydrating system 2. Theoretical analysis: *Journal of Geophysical Research* v. 102, p. 841-852.